Resonant multigap superconductivity at room temperature near a Lifshitz topological transition in sulphur hydrides

Maria Vittoria Mazziotti and Roberto Raimondi
Dipartimento di Matematica e Fisica, Università Roma Tre, via della Vasca Navale 84 00146 Roma, Italy

Antonio Valletta
Italian National Research Council CNR, Institute for Microelectronics and Microsystems IMM, via del Fosso del Cavaliere, 100, 00133 Roma, Italy

Gaetano Campi
Institute of Crystallography, CNR, via Salaria Km 29.300, I-00016 Montelibretti, Roma, Italy

Antonio Bianconi
RICMASS Rome International Center for Materials Science, Superstripes Via dei Sabelli 119A, 00185 Roma, Italy
Institute of Crystallography, CNR, via Salaria Km 29.300, I-00016 Montelibretti, Roma, Italy and
National Research Nuclear University MEPhI (Moscow Engineering Physics Institute), 115409 Moscow, Russia

The maximum critical temperature for superconductivity in pressurized hydrides appears at the top of superconducting domes in T_C versus pressure curves at a particular pressure, which is not predicted by standard superconductivity theories. Filling this gap we propose first-principles quantum calculation of a universal superconducting dome where T_C amplification in multigap superconductivity is driven by the Fano-Feshbach resonance due to configuration interaction between open and closed pairing channels, i.e., between multiple gaps in the BCS regime, resonating with a single gap in the BCS-BEC crossover regime. We focus on the a high-order anisotropic van Hove singularity near the Fermi level observed in band structure calculations of pressurized sulfur hydride, typical of a supermetal, associated with the array of metallic hydrogen wires modules forming a nanoscale heterostructure at atomic limit called superstripes phase. In the proposed three dimensional (3D) phase diagram the critical temperature shows a superconducting dome where T_C is a function of two variables (i) the Lifshitz parameter (η) measuring the separation of the chemical potential from the Lifshitz transition normalized by the inter-wires coupling and (ii) the effective electron phonon coupling (g) in the appearing new Fermi surface including phonon softening. The results will be of help for material design of room temperature superconductors at ambient pressure.

INTRODUCTION

Pressurized sulphur hydride H_3S with T_C=203 K at 162 GPa, [1] has reached in 2015 the record for the highest critical temperature, held before by cuprate perovskites since 1986 [2,3,4]. This discovery has been followed by superconductivity in lanthanum hydrides with T_C above 260 K [5,6], in yttrium hydrides with T_C = 243 K [7,8], and in a ternary carbonaceous sulfur hydride CSH_x [9] reaching room temperature. X-ray diffraction using focused synchrotron radiation has shown the crystalline $Im\bar{3}m$ lattice symmetry of H_3S above 103 GPa [10–13] and X-ray absorption spectroscopy has provided information on local structure of yttrium hydrides [14]. Recent experimental results show an anomalous superconductivity phase [7,8], while conventional superconductivity [15,16] considering only the pairing of the superconducting electrons via electron phonon coupling (Cooper pairs) and a single-gap superconductivity paradigm has been used to predict and to explain the high critical temperature in pressurized hydrides since the early days [17–21].

The paradigm shift to multi-gap superconductivity including the key role of Majorana exchange interaction between different condensates [22,23,24] has been proposed [25]. The old single-gap paradigm was found to be incompatible with band structure calculations of H_3S in the pressure range where the critical temperature shows its maximum value, T_{Cmax}. In fact band structure calculations [25–27], show that:

(i) the applied pressure induces an increasing compressive lattice strain which pushes an incipient density of states (DOS) peak, due to a van Hove singularity (vHS), to higher energy and it crosses the Fermi level, [25] which has been confirmed by several authors [28,29],

(ii) multiple Fermi surfaces coexist in different spots of the k space, [26],

(iii) the Migdal approximation $E_{Fn} \gg \hbar\omega_0$ in the appearing nth Fermi surface spot breaks down near the Lifshitz transition [27] ,

(iv) the anomalous pressure dependent isotope coefficient [27] strongly deviates from the single-band constant value predicted by standard BCS theory.

The Fermi energy E_{Fn} in the appearing new nth Fermi surface spot at the Lifshitz transition and the energy width of the vHS singularity are of the order of the energy

of the optical phonon $\hbar\omega_0$=160 meV observed by Capitani et al.[30] in pressurized H_3S infrared spectra which shows a Fano-lineshape with the characteristic strong asymmetry indicating its interference with electronic degrees of freedom at the Fermi level. [31,32]

The van Hove singularity (vHS) has been assigned by using band structure calculations to an electronic band of s orbitals due to the network of hydrogen chains with short $H-H$ hydrogen bonds [27]. The lattice compressive strain due to increasing pressure induces the energy shift of the vHS which crosses the chemical potential giving a Lifshitz transition for the appearing of a new small Fermi surface spot [25] while other Fermi surfaces contribute to the featureless weak broad background of the density of states. The Lifshitz transition belongs to the class of electronic topological transitions [33–36] for the appearing of a new Fermi surface which are 2.5 order stress induced transitions for non interacting Fermi gas but these transitions become first order transitions showing arrested phase separation for strongly interacting fermions [37,38]

The proposed scenario of multigap superconductivity near a Lifshitz transition in pressurized H_3S [26] was previously proposed by Bianconi, Perali and Valletta (BPV) for other non BCS superconductors like for hole doped cuprates [39–43], for diborides [22, 44–47], for iron doped superconductors [48–52], for organics [53 and 54] for metallic nanoscale multilayers with nodal lines where spin-orbit interaction plays a key role in T_C amplification [55]. for superconductivity [56] at interface of oxide perovskites which can host also Majorana fermions [57]. The BPV theory focuses on quantum Fano-Feshbach resonance which is a fundamental resonance in quantum mechanics due to configuration interaction between the open and the closed scattering channels [22,23,24]. The Fano-Feshbach resonance was first proposed theoretically in atomic physics by Fano in 1935 [31,32] and extended by Feshbach in 1962 in many-body physics of nuclear matter [58] where it is called shape resonance and it is described by the multi-channel optical model. This resonance has to be considered as the interaction varies from short to long time involving states of the system in which a part of the system is in the continuum.

In quantum theory of many body systems made of different electronic components the Fano-Feshbach resonances appear in systems where the Fermi wavelength of one of the components is of the order of the system size like in nuclear matter [59,60] and in condensed matter at nanoscale [61]. Shape resonances have been found in the final states of x-ray absorption near edge structure where the photoelectron wavelength is of the order of interatomic distance and the electronic multiple scattering resonance is degenerate with the continuum [62–64]. The exchange interaction between condensates was included in theories for overlapping band by Suhl, Matthias, and Walker (SMW) [65], Moskalenko [66] and Kondo [67] but

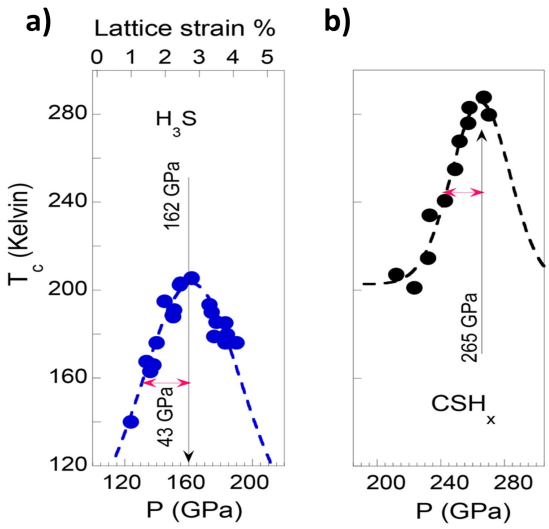

Figure 1. Panel **a**: The superconducting *dome* of H_3S for $P > 120\ GPa$ with the critical temperature $T_{Cmax} = 203K$ at its top at $P_{opt} = 162\ GPa$ with half width of about 43 GPa. Panel **b**: The superconducting *dome* of CSH_x for $P > 220\ GPa$ with $T_{Cmax} = 287K$ at $P_{opt} = 265\ GPa$

they assumed in a first approximation that all intraband pairing channels in each of the n bands are in the BCS regime with ($E_{Fn} \gg \omega_0$) and the exchange term for interband pair transfer was assumed to be a constant parameter with no energy or momentum dependence therefore the theories of overlapping bands did not include Fano-Feshbach resonances. The Fano-Feshbach resonance In the Bogoliubov superconductivity theory of multigap superconductors is due to configuration interaction between different pairing channels in different Fermi surfaces [68] with exchange of pairs between first condensates in the BCS regime and second condensates in the BCS-BEC crossover where the momentum and energy dependence of the exchange interaction between different coexisting gaps plays a key role while it is neglected in anisotropic Eliashberg theory of multigap superconductors. On the contrary, in the BPV theory [39] the Fano-Feshbach resonance between a *first* pairing channel (called closed channel) in the BCS-BEC crossover regime and the open pairing channels (called open channels) in other large Fermi surfaces in the BCS regime has been calculated from the overlap of the wave-functions of the electron pairs in different bands determined by the subtle overlap of the wave-functions of pairs in superlattices of interacting 1D or 2D units. In ultracold fermion gases the Fano-Feshbach resonance has been applied in 2004 to generate unconventional fermion superfluids with a very large ratio of T_c/T_F [69,70]. The quantum amplification mechanism at Fano-Feshbach resonance near a Lifshitz transition is generated by the

quantum interference of pairing between: (i) electrons in the new appearing small Fermi surface with low Fermi energy and Fermi wavelength λ_F of the order of the system size with (ii) electrons in other Fermi surfaces with very high Fermi energies and very short Fermi wavelength λ_F. At optimum T_C in the closed pairing channel, λ_F is larger but close to the superconducting coherence length $k_F\xi_0 \sim 10$ [71,72].

Here we propose that the experimental superconducting *dome* given by the curves of the critical temperature T_C as a function of pressure P in Fig.1 in sulfur hydrides are the smoking gun of the Fano-Feshbach resonances between pairing channels driven by the variable lattice strain [39,53,73] which tunes the chemical potential at a topological Lifshitz transition. In fact panel (a) of Fig.1 shows that the external pressure induces a compressive strain of the crystalline lattice constant $\epsilon = 100(a - a_0)/a_0$, where a_0 is the lattice constant at $P = 103\ GPa$ where a structural phase transition the $Im\bar{3}m$ lattice symmetry appears. The superconducting *dome* over the strain range $0.5 < \epsilon < 4$ shows the maximum T_C at $\epsilon = 2.5$. Panel b of Fig.1 shows that the width of superconducting *dome* observed in CSH_x [9] is more narrow than the width of H_3S *dome* and the maximum T_C is higher.

The Fano-Feshbach resonance in multigap superconductivity in H_3S, is supported by the unusual behavior of the isotope coefficient. Indeed, the isotope coefficient decreases from 2.37 to 0.31 in the range going to the threshold to the top of the superconducting *dome* [6, 27, 74, and 75] deviating markedly from 0.5 predicted by the single band BCS theory. A similar anomalous behavior of the isotope coefficient has been found in the superconducting *dome* of cuprate perovskites [76],[41],[43,51].

A nanoscale heterostructure is expected to appear in compounds made of multiple elements in combination which include ordering in the lattice and electronic degrees of freedom. In pressurized hydrides the nanoscale heterogeneity is determined by local lattice structure controlled by the effects of the lattice strain resulting from the interplay between lattice misfit-strain (or chemical pre-compression) and the external pressure. The materials show the realization of supersolid phase or superstripes phase where condensates made of multiple different itinerant and localized electronic states move in a low dimension, 1D or 2D, nanoscale heterostructure. In pressurized hydrides hydrogen atoms in the crystalline unit cell form nanoscale units, metallic wires, with a complex impelling order including those originating from either the nuclear (i.e., nanoscale lattice symmetry) and electronic symmetries.

The superconductivity in the superstripes phase with coexisting different localized and delocalized electronic components moving in complex nanoscale heterostructures of low dimensional (quasi one.dimensional 1D)

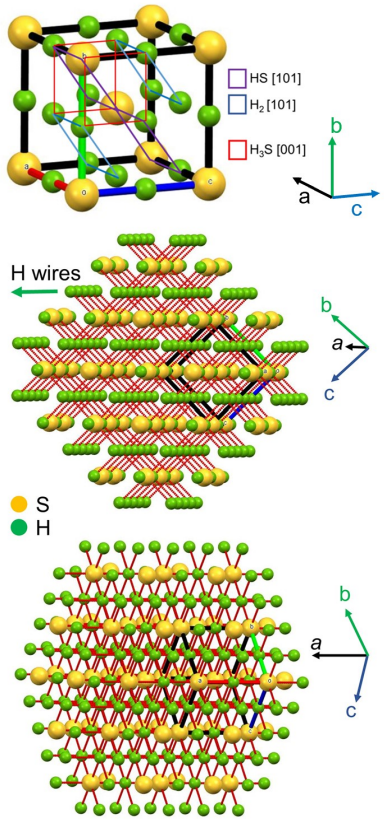

Figure 2. The upper panel shows the unit cell of pressurized H_3S crystal structure at 150 GPa with cubic $Im\bar{3}m$ lattice. The central and lower panels show that at mesoscale H_3S appears to be made of stacks of H_2 layers (small green dots) in the [101] plane intercalated by HS layers where S is indicated by large yellow dots. The central projection of the H_3S crystal shows that the H_2 layers are made of atomic hydrogen chains with the shortest H-H metallic bonds in the [100] direction.

structural units : called chains or stripes or ladders has been found in

i) A15 intermetallics which have held the record as having the highest superconducting critical temperature of 23.2 K from 1973 to 1986. A15 intermetallics like Nb_3Ge and Nb_3Sn have the same average crystal symmetry $Im\bar{3}m$ as H_3S [68] and show complex textures made of a 3D network of interacting 1D metallic Nb chains [77]. ii) hole doped cuprate perovskites where 2D networks of extrinsic stripes with different local lattice distortions [78–80] appear at nanoscale in the CuO_2 atomic layers facilitated by the polymorphism of perovskite structures which form metamorphic lattice stripes in mismatched material systems [81] which is tuned by the lattice misfit strain [73,82,83], iii) superconducting organics like doped p-terphenyl [54] where 1D-wires of short hydrogen bonds have been observed by X-ray diffraction [84] and it was proposed that the high-T_C is driven by Fano-Feshbach

resonance in the nanoscale superlattice of quantum wires [53].

Superlattices of two-dimensional (2D) metallic quantum wells at nanoscale have been found in: *i*) diborides made of stacks of boron layers intercalated by magnesium [85–89],

ii) iron-based perovskite superconductors, isostructural with electron doped cuprates, [90,91], are made of stacks of iron atomic layers and the tuning of the chemical potential near the Lifshitz transition have been clearly seen in ARPES experiments [52,92,93], tuned by misfit strain and doping at optimum doping

In this work we present the theoretical prediction of the superconducting dome for room-temperature superconductivity in pressurized hydrides due to a Fano-Feshbach resonance in multigap superconductivity near a Lifshitz transition in the frame of the multigap superconductivity scenario discussed recently by several authors [94–105]. A key feature of our approach is the calculation of exchange integrals, obtained by the overlap of the wave-functions of electrons in different Fermi surfaces calculated by solving the Schroedinger equation for a lattice heterostructure including the renormalization of the chemical potential at the Lifshitz transition with the opening of a new superconducting gap, controlled by constraints of the density equation. The results provide a significant step in understanding room-temperature superconductivity and the physical origin of the superconducting *dome*. Moreover, we propose a road map for the material design of artificial mesoscopic heterostructures made of nanoscale quantum wires which can be used by material scientists to synthesize new room-temperature superconductors at ambient pressure.

THE HETEROSTRUCTURE AT ATOMIC LIMIT: SUPERSTRIPES PHASE

According to the claims in the patents [106,107], we propose the material design of a heterostructure at atomic limit made of a nanoscale superlattice of weakly interacting quantum wires [108] which shows the multicomponent electronic structure in the energy window of the cut-off of the pairing interaction as in pressurized hydrides. Here we propose the design of a heterostructure at atomic limit made of superconducting quantum wires running in the x-direction intercalated by spacers of thickness W with periodicity $d = W + L$ (in the z-direction). The metallic wires are separated by spacers which generate a potential barrier. of amplitude V. Although the proposed nanoscale heterostructure is an oversimplification with respect to the real crystal structure shown in Fig.2, nevertheless it provides a heterostructure which is able to capture the main features of the DOS at the van Hove singularity near the Fermi level

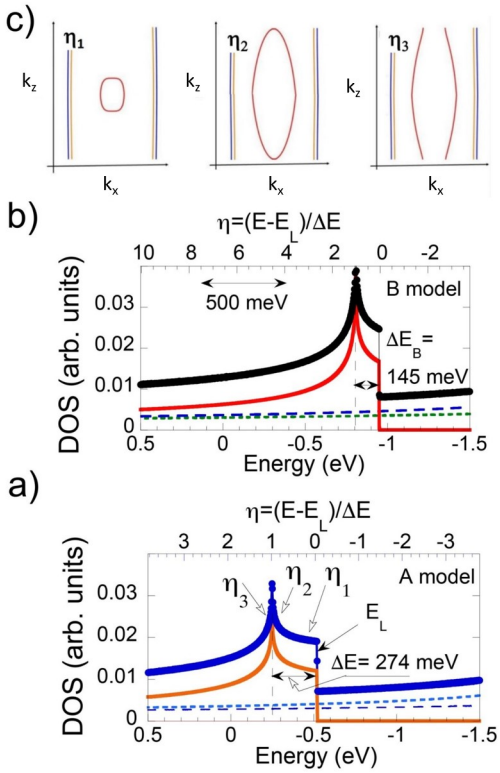

Figure 3. *Bottom panels*: total Density of States (DOS) for the case A, panel **a** (for the case B, panel **b**) shown by the thick solid blue (black) line as a function of the Lifshitz parameter η of the superlattice of quantum wires with weak inter-wire interaction giving the transversal dispersion $\Delta E = 274\ meV$ $(145\ meV)$. The figure shows also the high partial DOS curves at the van Hove singularity due to the upper third subband (red line) with small Fermi energy and the low partial DOS curves due to first and second subbands (blue dashed lines) with high Fermi energies. The top panel **c** shows the Lifshitz topological transition in the Fermi surfaces due to the third subband, shown with a solid red line, where the Fermi surfaces for the first and second subbands are indicated by blue and orange lines. The appearing Fermi surface due to the third subband changes at three different values of η indicated in panel **a**: η_1 corresponds to the appearing of a small tubular Fermi surface in the k_x, k_z plane; η_2 is the energy where the size of the tubular Fermi surface becomes large and it is close to the Lifshitz transition for neck disrupting (opening a neck) where its topology changes from 2D for η_2 to 1D for η_3 [25].

of H_3S. This heterostructure is a particular case of a supersolid stripes crystal [109] called superstripes [52 and 110]. which can be realized with optical lattices in ultracold gases [111]. The lineshape of the DOS peak shows the features of a high-order anisotropic van Hove singularity typical of a supermetal [112], In this superstripes phase the superconductivity is calculated using the BPV

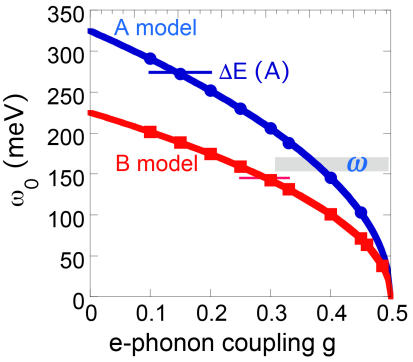

Figure 4. The softening of the phonon energy $\tilde{\omega}_0$ according to the Migdal theory, as a function of the intraband electron-phonon coupling g in the small Fermi surface spot appearing at the Lifshitz transition for the case A (blue line) and for the case B (red line)

approach first proposed for striped cuprate perovskites [39–43, 76, and 113].

We present numerical calculations of multigap superconductivity *dome* of the critical temperature as a function of pressure where we change both *i*) the proximity of the chemical potential from the Lifshitz transition, *ii*) the electron-phonon coupling for electrons in the upper subband and the *iii*) the phonon softening for increasing electron-phonon coupling g in the disappearing Fermi surface.

The proximity to the Lifshitz transition is measured by the Lifshitz parameter η given by the energy difference between the chemical potential and the energy E_L of the topological Lifshitz transition, which is the band-edge energy of the highest energy subband, normalized to the transversal energy dispersion, ΔE, between the 1D metallic chains

$$\eta = \frac{\mu - E_L}{\Delta E}.$$

The applied external pressure induces the variation of either *i*) of the Lifshitz parameter η and *ii*) of the electron-phonon coupling joint with phonon energy softening of the particular phonon mode coupled with the electrons in the small Fermi surface spot in the new appearing subband. In the heterostructure of quantum wires the electrons along the x-direction are free, while along the z-direction they are subjected to a periodic potential. Hence, the eigenfunctions $\psi_{nk_z}(z)$ and the eigenvalues $E_n(k_z)$, along the confinement direction, can be computed only numerically by solving a corresponding Kronig-Penney model. The solution of the eigenvalues equation gives the electronic dispersion for the n subbands. Indeed, in the heterostructure of quantum wires, the quantum-size effects give a multiband electronic structure where the subband with higher energy shows a two-dimensional behavior due to hopping between 1D-chains. For the numerical calculation of the superconducting dome of H_3S we start with the evaluation of the DOS peak in [27] at E_F by using a model of 1D-chains corresponding to the chains with short H-H bonds, as shown in Fig.2. We have designed an artificial nanoscale heterostructure at atomic limit made of quantum wires which reproduces the van Hove singularity (vHS) of H_3S calculated by band structure calculations [27] in a range of 500 meV around the Fermi energy i.e., within the energy cut-off of the pairing interaction relevant for the emergence of superconductivity. We consider two models (A and B) for the heterostructure made of stripes of width $L = 0.85$ nm, spacers of width $W = 0.55$ nm separated by a potential barrier V characterized by two different coupling between the quantum wires. The model A for the case of higher inter-wires coupling is characterized by a transversal dispersion energy ΔE= 274 meV as it was found in H_3S, while model B for the case of smaller inter-wires coupling is characterized by a smaller transversal dispersion $\Delta E = 145$ meV, which is expected to give a sharper superconducting *dome* and a higher maximum critical temperature reaching room temperature. The DOS peak of the vHS and the partial DOS for the model A and model B as a function of the Lifshitz parameter are plotted in panel (a) and panel (b) of Fig.3 respectively. Panel (c) of Fig.3 shows the Lifshitz transition for the appearing of a new Fermi surface, called of type (I), tuning the chemical potential near the band-edge (η_1) of the subband with a critical point where a new 2D Fermi surface spot appears. The second type of Lifshitz transition (type II) occurs at the opening of a neck (or neck disrupting) in the small Fermi surface with the appearing of a singular nodal point which gives the sharp DOS maximum at η_2 (Fig.3 panel (c)) at the crossover between the 2D and 1D topology. The nearly flat portion of the DOS between (type I) and (type II) Lifshitz transitions in Fig.3 correspond with the regime where a small 2D Fermi surface with a low Fermi energy appears. While in previous theoretical descriptions of the Fano-Feshbach resonance near the Lifshitz transition the electron-phonon coupling g_{nn} was assumed to be constant, in this work we take into account that the external pressure changes either the Lifshitz parameter (η) and the electron-phonon coupling g_{nn} in the appearing Fermi surface in the upper subband and the renormalized phonon energy $\tilde{\omega}_0$ shows the softening according to the *Migdal relation*:

$$\tilde{\omega}_0 = \omega_0 \sqrt{1 - 2g}. \quad (1)$$

The relation contains the coupling constant for the metal forming the superconducting layers for $g < 0.5$, and it is used here to qualitatively estimate the effect of the coupling constant on the phonon frequency in the appearing Fermi surface as it is shown in Fig.4. In our theory, the variable $\tilde{\omega}_0$ is also the cut-off energy of the pairing in-

teraction in the Bogoliubov gap equation which changes with η. We have fixed, for the case A, $\omega_0 = 330\ meV$ in order to reproduce with moderate intraband electron phonon coupling, $0.3 < g < 0.33$, the experimental phonon frequency, $\tilde{\omega}_0 = 160\ meV$ [30], measured in pressurized H_3S at 150 GPa For the case B we have fixed $\omega_0 = 225\ meV$, in order to get $\tilde{\omega}_0 = \Delta E = 145\ meV$ with moderate intraband electron phonon coupling $g = 0.25$.

In the case of organic superconductors [53] it has been shown that the amplification of the critical temperature in heterostructures of quantum wires and a narrow superconducting dome occurs where the coupling in the appearing new nth Fermi surface is larger than the in other Fermi surfaces and the interband coupling is small. In our model $g_{nn'}$ is the superconducting dimensionless coupling constant for the three-band system which has a matrix structure that depends on the band indices n and n'.

In this work we confirm previous results [53]: in fact the superconducting dome with a sharp drop of T_C at both sides of the maximum with a stronger Fano-Feshbach anti-resonance is generated by a weak intraband coupling for the Cooper pairing channel g_{nn} and weak inter-band exchange channels $g_{nn'}$. The Fano-Feshbach resonance increases the maximum value of T_C at the top of the *dome* increasing the intra-band coupling for the Cooper pairing channel g_{nn} in the new appearing or disappearing Fermi surface.
Moreover the maximum of the critical temperature is expected to increase where the phonon energy giving the energy cut off for the pairing processes is of the same order as the hopping energy between the wires $\Delta E = \tilde{\omega}$.

When the Lifshitz parameter is tuned between the band-edge and the van Hove singularity, a new Fermi surface appears with a very small number density of electrons in the strong coupling limit. The condensates in the other Fermi surfaces (first and second subband) have a very high Fermi energy and therefore are in the adiabatic regime and coexist with a third condensate in the small Fermi surface where the classical BCS approximations are violated. In the models (A) and (B) for $0<\eta<1$ a new closed 2D Fermi surface appears as shown in band structure calculations [25] for H_3S around 160 GPa where the maximum critical temperature is observed at a top of a *dome*. For this heterostructure we assume that quantum size effects are not negligible and the electron hopping in the transverse direction is finite so that the quantum wires can be considered weakly interacting This is reflected in the spectrum that appears to split into n subbands characterized by quantized values of the transverse moment that depends on the band index and the dimension of the wires.

In the heterostructure of quantum wires the electrons along the x-direction are free, while along the z direction they are subjected to a periodic potential $V(z)$:

$$V(z) = V\sum_{-\infty}^{\infty}\theta(W/2 - |m\lambda_p - z|). \tag{2}$$

In the periodic potential we assume that the full single-particle wave-function can be written as

$$\psi_{n,\mathbf{k},\alpha}(\mathbf{r}) = \frac{1}{\sqrt{L_x L_z}} e^{ik_x x}\psi_{nk_z}(z)\boldsymbol{\chi}_\alpha, \tag{3}$$

where L_x and L_z are the spatial dimensions of the system, n is the band index, $\mathbf{k} = (k_x, k_z)$ is the wavevector, and $\boldsymbol{\chi}_\alpha$ is the spinor part with spin $\alpha =\uparrow$ or $\downarrow$. The corresponding energy eigenvalues, independents from the spin, are given by

$$\varepsilon_n(\mathbf{k}) = \frac{\hbar^2}{2m_x}k_x^2 + E_n(k_z). \tag{4}$$

The eigenfunctions $\psi_{nk_z}(z)$ and the eigenvalues $E_n(k_z)$ are computed numerically by solving a corresponding Kronig-Penney model. The solution of the eigenvalues equation gives the electronic dispersion for the n subbands.

MULTIGAP SUPERCONDUCTIVITY BEYOND BCS

In the multigap superconducting scenario the exchange integral for pairs of electrons in different bands plays a key role for the T_C amplification while it is neglected in the single-band BCS theory. The exchange interaction is not constant but depends not only on the wave vector along z but also on the band index, therefore it has a matrix structure

$$U^{nn'}_{k_z k'_z} = -\frac{U_0}{2}\int_S |\psi_{nk_z}(z)|^2|\psi_{n'k'_z}(z)|^2 dz = -\frac{U_0}{2}I^{nn'}_{k_z k'_z}, \tag{5}$$

where $I^{nn'}_{k_z k'_z}$ is the pair superposition integral, calculated considering the interference between electronic wave functions in different subbands. The non diagonal pairing terms (nm) due to the exchange interaction calculated for model A are shown in Fig.5. The self-consistent equation for the superconducting gap at zero temperature can be written as

$$\Delta_{nk_z} = -\frac{1}{2M}\sum_{n',\mathbf{k'}}\frac{U^{nn'}_{k_z k'_z}\Delta_{n'k'_z}}{\sqrt{(E_{n'}(\mathbf{k'}) - \mu)^2 + |\Delta_{n'k'_z}|^2}}, \tag{6}$$

where M is the total number of wavevectors.

In order to take into account the renormalisation of the chemical potential and charge densities in each subband when a new superconducting gap appears in a single subband, the joint Bogoliubov gap equation and the charge

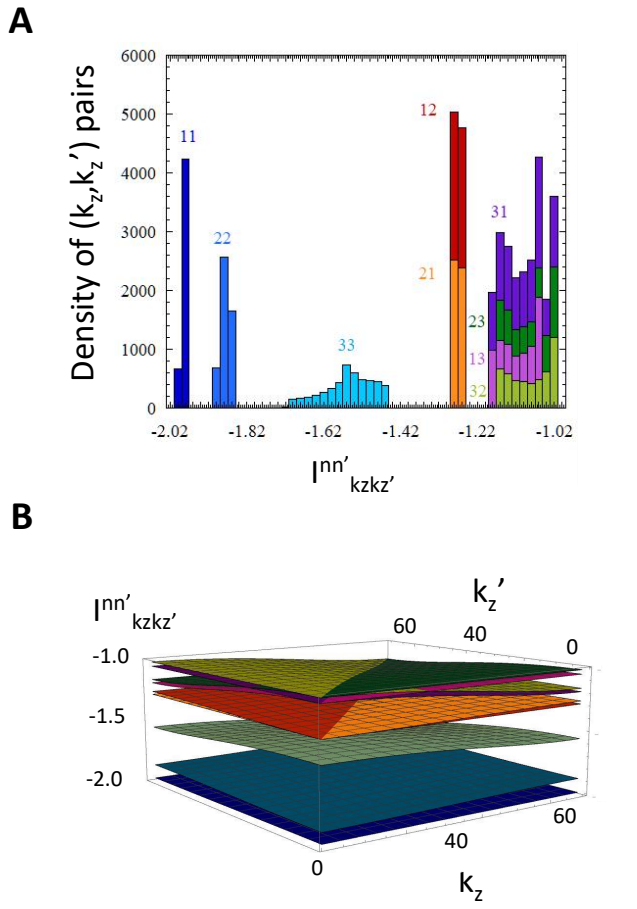

Figure 5. *Panel* **A**: histogram of the superposition integral of equation (5). The numbers indicate the different elements of the matrix of the intraband pairings $I^{n,n'}_{k_z k'_z}$ and the interband couplings $I^{n,n'}_{k_z k'_z}$. *Panel* **B**: the matrix elements of the exchange integral as a function of the wavevectors in the direction of the confinement potential. The colors correspond to those of the histogram.

density equation have been solved where the charge density ρ and the chemical potential in the superconducting phase are related by

$$\rho = \frac{1}{S}\sum_{n}^{N_b}\sum_{k_x,k_z}\left(1-\frac{E_n(k_x,k_z)-\mu}{\sqrt{(E_n(k_x,k_z)-\mu)^2+\Delta^2_{n,k_z}}}\right), \quad (7)$$

In this equation the dispersion along k_x is parabolic, N_b is the number of the occupied subbands. The joint solution of the gap equation (3) and the density equation (4) is essential in order to correctly describe the multigap superconductivity near the Lifshitz transition where the gap in the upper subband approaches to the Bose-Einstein condensation.

The superconducting critical temperature is calculated by iteratively solving the linearized equation

$$\Delta_{n\mathbf{k}} = -\frac{1}{2M}\sum_{n'\mathbf{k'}} U^{nn'}_{k_z k'_z}\Delta_{n'k'_z}\frac{\tanh\left(\frac{(E_{n'}(\mathbf{k'})-\mu)}{2T_C}\right)}{(E_{n'}(\mathbf{k'})-\mu)} \quad (8)$$

until the vanishing solution is reached with increasing temperature.

Here we present a case of Fano-Feshbach resonant superconductivity giving a superconducting *dome* where the top of the *dome* reaches the high temperature range $200 < T_c max < 300K$ of pressurized hydrides much larger than $T_c max = 123K$ calculated in a previous work for cuprates and organics [53]. This result is obtained by the resonance regime by increasing gaps anisotropy where the two gaps differ by a sizable factor in the range 2.9-3.9, at the top of the dome where the coupling strength in a small Fermi surface spot is in the range $0.3<g<0.42$ and the phonon energy scale determines not only a large prefactor for the critical temperature, but it also induces a large width of the resonance.

Here following Ref.[53] the superconducting dome is generated by considering the case where the first and the second subband being in a weak coupling regime, *i.e.*, we use for dimensionless coupling constants the following values: $g_{11} = g_{22} = 0.1$, while we change the coupling in the third subbands $g_{33} = g$, in the range of values between 0.10 and 0.49, and in parallel we vary the cut-off energy, ω_0 according to the Migdal relation [114].

In Fig.6 the panel A1 (B1) shows the values of the gap ratio, $2\Delta/T_C$, for the second and third subband for the A (B) case as a function of the Lifshitz parameter η. The panel A2 (B2) in Fig.6 shows the trend of the isotope coefficient for the A (B) case as a function of the Lifshitz parameter η. All these graphs were obtained at a fixed coupling value equal to $g = 1/4$ for the case (A) and at $g = 1/3$ for the case (B). At the Lifshitz transition for the appearing of a new Fermi surface, $\eta = 0$, the value of the gap ratio $2\Delta/T_C$ is close to the predicted value the BCS theory ($2\Delta/T_C = 3.5$) but for $0.5 < \eta < 1 = 0$ we see strong deviations from the BCS single gap prediction. In fact, $2\Delta_2/T_C$ reaches a very small value, between 0 and 1, while $2\Delta_3/T_C$ remains approximately constant at the BCS value. A similar scenario was observed in magnesium diboride [48] due to the exchange integral for pairs transfer between the second and third subbands.
While the BCS theory predicts that the isotope coefficient should be constant close to the value of 0.5 we see that the isotope coefficient shows a strong maximum of the Lifshitz transition $\eta = 0$, and a minimum at $0.5 < \eta < 1 = 0$ near the topological Lifshitz transition for opening a neck in the Fermi surface of the third subband, These theoretical predictions are in agreement with the experiments showing that the isotope coefficient shows an anomalous trend as a function of pressure in pressurized sulfur hydrides [27]. I

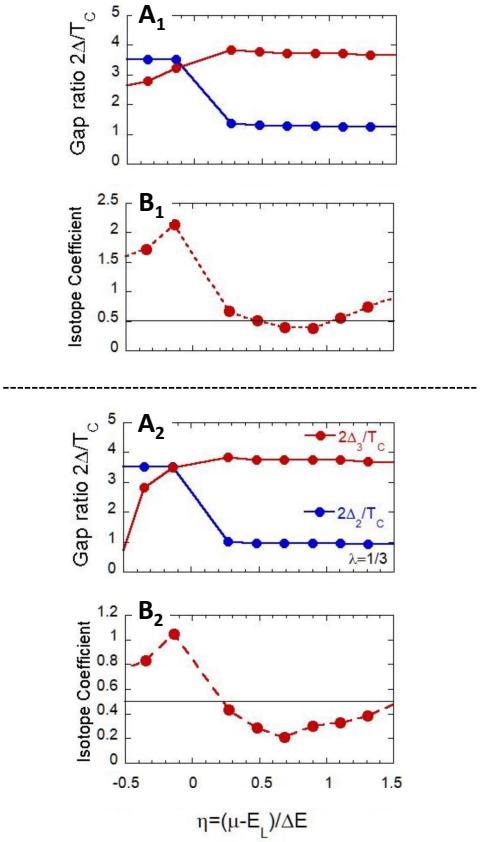

Figure 6. *Panel* $\mathbf{A_1}$: gap ratio as a function of the Lifshitz parameter for $g = 1/4$ (case (A)) for the second and third subband. *Panel* $\mathbf{B_1}$: isotope coefficient as a function of the Lifshitz parameter for $g = 1/4$ (case (A)). *Panel* $\mathbf{A_2}$: gap ratio as a function of the Lifshitz parameter for $g = 1/3$ (case (B)) for the second and third subband. *Panel* $\mathbf{B_2}$: isotope coefficient as a function of the Lifshitz parameter for $g = 1/3$ (case (B)).

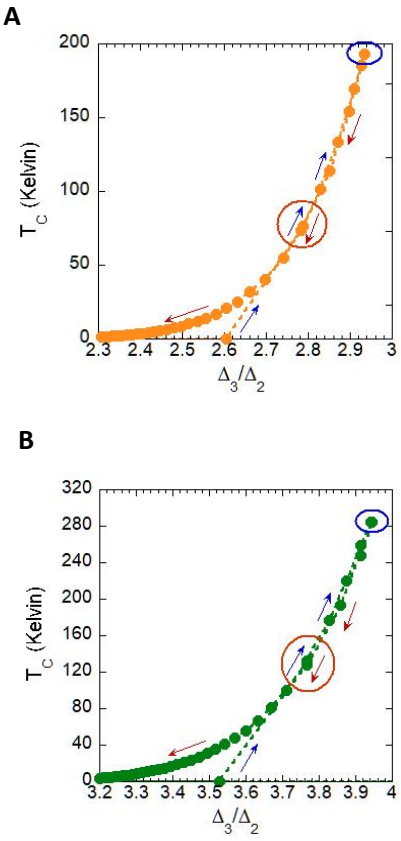

Figure 7. The critical temperature as a function of the ratio between the gap in the third subband and the gap in the second subband. Panel **A** represents the trend for the case (A), while panel **B** represents the case (B). It can be noted that in the range $2.6 < \Delta_3/\Delta_2 < 2.9$ (for the case (A)) or $3.5 < \Delta_3/\Delta_2 < 3.9$ (for the case (B)) the critical temperature increases as the anisotropy between the gaps increases (blue arrows) until it reaches a maximum value when Δ_3/Δ_2 is maximum, from this point on then the T_C decreases almost exponentially as the ratio between the gaps decreases (red arrow). The blue circle represents the point where T_C is maximum, the red circle the point of intersection of the two opposite trends.

In Fig.7 we show the trend of the critical temperature as a function of the ratio between the gap in the third subband and the gap in the second subband for the case A in panel A and for the case B in panel B. The results clearly show that the maximum critical temperature is reached with the highest anisotropy between the gaps. In fact the graph shows that the maximum of T_C is reached when the ratio Δ_3/Δ_2 is maximum. This figure shows clearly that room-temperature superconductivity is reached by increasing electron-phonon coupling in the a small Fermi surface spot pushing up the gap in the appearing Fermi surface due to the third subband Δ_3 while the gap Δ_2 in the second Fermi surface with large Fermi energy remains small because the electron-phonon coupling remains small. These results show the predicted effect of Fano-Feshbach resonance driven by the exchange interaction between closed (strong) pairing channels in the third subband and open (weak) pairing channels in the second subband

SUPERCONDUCTING DOME

In Fig.8 we plot the critical temperature as a function of the Lifshitz parameter in both semi-logarithmic and linear scales for variable values of the electron-phonon (e-ph) coupling in the upper subband. In the linear scale we see a variable superconducting dome where $T_C max$ increases with g increasing up to $g = 0.4$ and it decreases in the range $0.4 < g < 0.5$ because of the phonon softening goes to zero at $g = 0.5$. In the case (A) the maximum value of the critical temperature is 250 K, therefore it

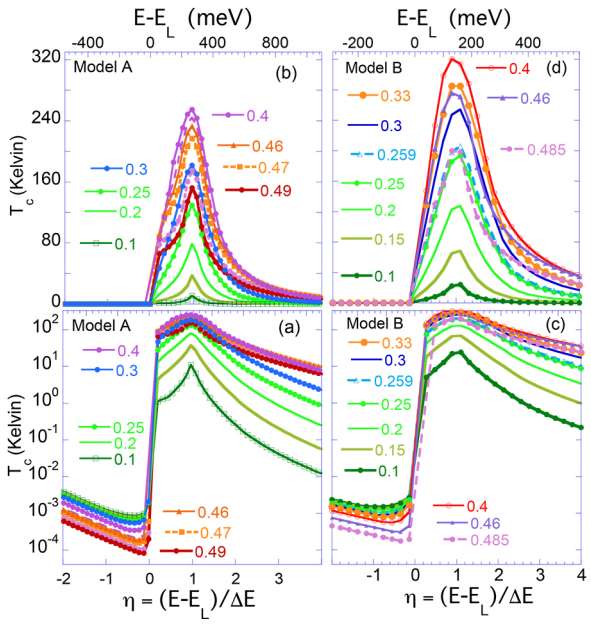

Figure 8. Critical temperature as a function of the Lifshitz parameter (horizontal axis at the bottom) and as a function of the energy with respect to the band-edge (horizontal axis at the top) as the electron-phonon coupling varies, for two different models: case A (left panels) and case B (right panels). The curves in the bottom panels are plotted in a linear scale to show the evolution of the superconducting dome and in a semi-log scale in top panels to show the suppression of the critical temperature due to the Fano antiresonance of the left side of the dome. This plot shows that the critical temperature T_C for case A reaches a maximum value of 250 K, while for case B it reaches a maximum value of 330 K.

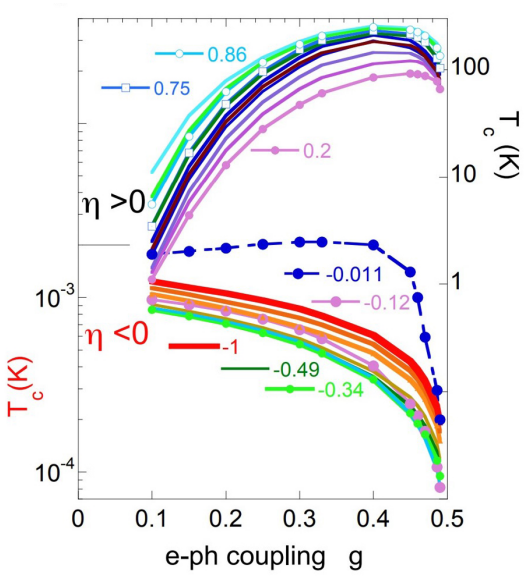

Figure 9. The critical temperature T_C as a function of the electron-phonon coupling g at fixed different Lifshitz parameters η for the case A. The curves $T_C(g)$ in the lower part of the figure show the case with fixed η in the anti-resonant regime $-1 < \eta < 0$ where the critical temperature *decreases* by increasing the electron phonon coupling g reaching a minimum at $\eta = -0.34$. The upper part of the figure shows the cases for $\eta > 0$ in the resonant regime, where the critical temperature *increases* by increasing g in the range $0.1 < g < 0.4$ with the temperature scale in the right side.

explain the superconductivity in H_3S. While the maximum T_C in case (B) reaches 330 K showing the possibility of room-temperature superconductivity. The graphs in semi-logarithmic scale show the typical form of the Fano-Feshbach anti-resonance which becomes more relevant as g increases. Fig.9 shows the variation of the critical temperature T_C at constant η and the variable electron-phonon coupling g for the A case. In the anti-resonant regime $-1 < \eta < 0$ we observe a clear feature of the Fano-Feshbach resonance. In fact at the low energy side of the Fano-Feshbach resonance between closed and open channels the negative interference gives the observed T_C minimum appearing at $\eta = -0.34$ where the critical temperature decreases with increasing e-ph coupling, on the contrary for $\eta > 0$ T_C increases with increasing e-ph coupling up to $g = 0.4$.

Fig.10 shows the critical temperature T_C(g,η) as a function of two variables: (i) the e-ph coupling in the third subband (g), where g is the reduced Allen-Dynes electron-phonon coupling ($\lambda/(1+\lambda)$) [16] and (ii) the Lifshitz energy parameter (η). The critical temperature T_C is calculated by BPV approach including the superconducting shape resonance between multiple gaps. The maximum T_C of the dome occurs in the (η, g) plane at the point $(1, 0.4)$ *i.e.*, at the Lifshitz transition for neck disrupting, at η=1, for *opening* a *neck* associated with a transition from 1D topology at higher energy to a 2D topology at lower energy of the small appearing Fermi surface. The *universal superconductive dome* obtained in this figure is needed to understand the experimental dome observed in the experimental curves of the critical pressure versus pressure T_C(P) of sulphur hydrides. In fact the external pressure induces a joint variation of both the energy position of the chemical potential with respect to the band-edge (the Lifshitz parameter η) as well as the electron-phonon coupling g in the upper subband along a line in the (η,g) plane. The variable electron-phonon coupling is associated with the softening of the phonon mode energy coupled with electrons in the upper subband according to the Migdal relation. Therefore the experimental curve of T_C *vs* pressure shown in Fig.1 for a

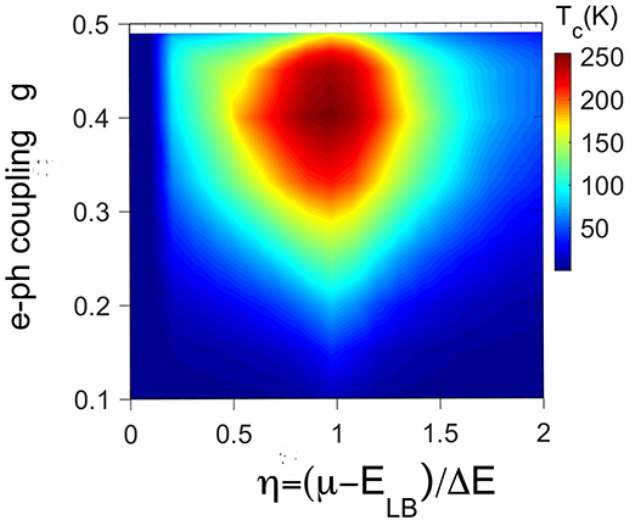

Figure 10. Calculated superconducting dome for H_3S simulated using the proposed A model. The critical temperature is plotted in a color plot from blue ($T_C = 0K$) to red ($T_C = 250K$) as a function of two variables controlling the pairing strength in the new appearing small Fermi surface above the band edge of the third upper subband: (i) the Lifshitz parameter η measuring the normalized Fermi energy E_{F3} in the range $0 < \eta < 2$ and (ii) the reduced Dynes [16] electron-phonon coupling g=(λ/(1+λ)) with lambda equal to the bare pair coupling.

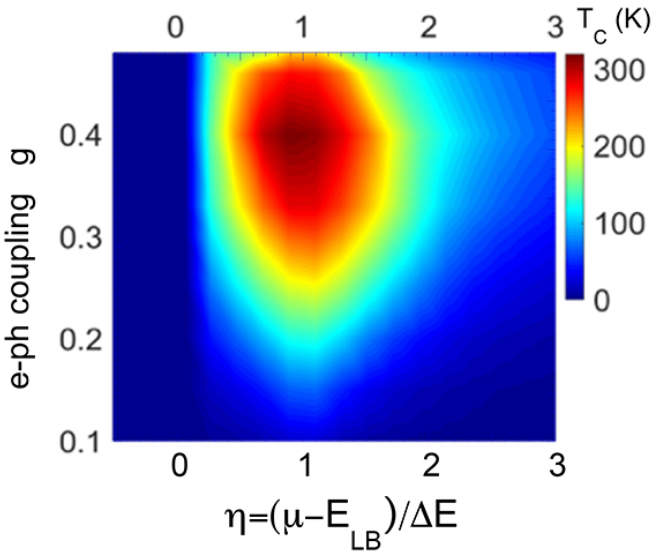

Figure 11. 3D color plot of T_C as a function of two variables (η, g) calculated using the BPV approach for the heterostructure B, proposed here as the B model for pressurized CSH_x. The critical temperature increases from blue ($T_C = 0$ K) to red ($T_C = 300$ K) in the (η,g) plane. The superconducting dome is due to the shape resonance between multiple superconducting gaps where the superconducting critical temperature reaches room temperature as shown in the color plot of (T_C) as a function of the Lifshitz parameter η and the electron-phonon coupling g in the appearing Fermi surface at the E_L energy of the Lifshitz transition The critical temperature reaches room temperature superconductivity where the multigap superconductor is close to a Lifshitz transition for neck disrupting with the Lifshitz parameter in the range $0.6 < \eta < 1$ and e-ph coupling close to 0.4.

particular pressurized hydride is determined by different cuts of the universal superconductive dome determined by the particular pathway in the (η,g) plane driven by variable pressure.

In order to reproduce room-temperature superconductivity in CSH_x we have numerically evaluated the gaps and critical temperature for the case (B) where we have decreased the hopping between the wires to simulate the modified spacer material in CSH_x in comparison with H_3S. Therefore we have used the transversal dispersion $\Delta E = 145$ meV to simulate the superconducting dome of CSH_x . The results are shown in Fig.10 and Fig.11. In the case B the critical temperature $T_C max$ at the top of the *superconducting dome* reaches room-temperature superconductivity.

Tuning the chemical potential, μ, in the proximity of the band-edge the superconducting system reaches different regimes which are distinguished by the Lifshitz parameter. At the Lifshitz transition for appearing of the new Fermi surface spot the Fermi level in the hot spot is very low and therefore the few electrons there are strongly coupled with lattice phonons showing the Khon anomaly and softening with superconductivity competing with charge density wave (CDW) and phase separation as it has been observed in doped diborides [85,88] which show phonon softening at maximum T_C [115].

In the Lifshitz transition for the topological transition of the type opening a neck the Fano-Feshbach resonance gives the maximum T_C. In fact the BCS condensates, made of the majority of electrons in the first subbands, coexist with a minority of electrons in the second subband forming a condensate in BCS-BEC crossover [94 and 116]. These results show that the maximum critical temperature in the multigap superconducting scenario can reaches room temperature superconductivity driven by exchange interaction between different condensates, neglected in the BCS approximations.

CONCLUSIONS

In conclusion, we have shown that the theory of multigap superconductivity in a superlattice of nanoscale stripes which was first proposed for high temperature superconductivity in hole doped cuprate perovskites [39–43], could provide a quantitative description of room temperature superconductivity in pressurized hydrides. We have calculated the superconducting domes for two dif-

ferent cases of the heterostructure of quantum stripes with larger and smaller hopping between stripes where the critical temperature is determined by both the Lifshitz parameter and the variable electron-phonon coupling in the appearing Fermi surface. The key point of our work is the solution of the Bogoliubov gap equations in a multigap system including the Fano.Feshbach resonance driven by the variable exchange interaction between condensates, which is usually neglected in standard Migdal-Eliashberg theory. We have shown that multiple gaps in large Fermi surfaces with high Fermi energy in the weak coupling regime can be amplified by exchange interaction with a large gap in the strong coupling regime in a small Fermi surface spot. We have presented cases where the Fano-Feshbach resonance appears by tuning the chemical potential near an electronic topological Lifshitz transition in heterostructures of quantum wires. We have presented two different heterostructures of quantum wires where the critical temperature reaches the $200 < T_c < 300K$ range.

We thank the staff of Department of Mathematics and Physics of Roma Tre University, the Computing Center of Institute of Microelectronics and Microsystems IMM of Italian National Research Council CNR and Supertripesonlus for financial support of this research project.

[1] A. Drozdov, M. Eremets, I. Troyan, V. Ksenofontov, and S. I. Shylin, Nature **525**, 73 (2015).
[2] J. G. Bednorz and K. A. Müller, Reviews of Modern Physics **60**, 585 (1988).
[3] L. Gao, Y. Xue, F. Chen, Q. Xiong, R. Meng, D. Ramirez, C. Chu, J. Eggert, and H. Mao, Physical Review B **50**, 4260 (1994).
[4] A. Yamamoto, N. Takeshita, C. Terakura, and Y. Tokura, Nature communications **6**, 1 (2015).
[5] M. Somayazulu, M. Ahart, A. K. Mishra, Z. M. Geballe, M. Baldini, Y. Meng, V. V. Struzhkin, and R. J. Hemley, Physical Review Letters **122**, 027001 (2019).
[6] A. P. Drozdov, P. P. Kong, V. S. Minkov, S. P. Besedin, M. A. Kuzovnikov, S. Mozaffari, L. Balicas, F. F. Balakirev, D. E. Graf, V. B. Prakapenka, *et al.*, Nature **569**, 528 (2019).
[7] I. A. Troyan, D. V. Semenok, A. G. Kvashnin, A. V. Sadakov, O. A. Sobolevskiy, V. M. Pudalov, A. G. Ivanova, V. B. Prakapenka, E. Greenberg, A. G. Gavriliuk, *et al.*, Advanced Materials **33**, 2006832 (2021).
[8] P. Kong, V. S. Minkov, M. A. Kuzovnikov, A. P. Drozdov, S. P. Besedin, S. Mozaffari, L. Balicas, F. F. Balakirev, V. B. Prakapenka, S. Chariton, *et al.*, Nature Communications **12**, 1 (2021).
[9] E. Snider, N. Dasenbrock-Gammon, R. McBride, M. Debessai, H. Vindana, K. Vencatasamy, K. V. Lawler, A. Salamat, and R. P. Dias, Nature **586**, 373 (2020).
[10] M. Einaga, M. Sakata, T. Ishikawa, K. Shimizu, M. I. Eremets, A. P. Drozdov, I. A. Troyan, N. Hirao, and Y. Ohishi, Nature physics **12**, 835 (2016).
[11] A. F. Goncharov, S. S. Lobanov, V. B. Prakapenka, and E. Greenberg, Physical Review B **95**, 140101 (2017).
[12] D. Duan, Y. Liu, Y. Ma, Z. Shao, B. Liu, and T. Cui, National Science Review **4**, 121 (2017).
[13] I. Kruglov, R. Akashi, S. Yoshikawa, A. R. Oganov, and M. M. D. Esfahani, Physical Review B **96**, 220101 (2017).
[14] J. Purans, A. Menushenkov, S. Besedin, A. Ivanov, V. Minkov, I. Pudza, A. Kuzmin, K. Klementiev, S. Pascarelli, O. Mathon, *et al.*, Nature Communications **12**, 1 (2021).
[15] G. Eliashberg, Sov. Phys. JETP **11**, 696 (1960).
[16] R. Dynes, Solid State Communications **10**, 615 (1972).
[17] D. Duan, Y. Liu, F. Tian, D. Li, X. Huang, Z. Zhao, H. Yu, B. Liu, W. Tian, and T. Cui, Scientific reports **4**, 6968 (2014).
[18] D. Duan, X. Huang, F. Tian, D. Li, H. Yu, Y. Liu, Y. Ma, B. Liu, and T. Cui, Physical Review B **91**, 180502 (2015).
[19] A. P. Durajski and R. Szczęśniak, Scientific Reports **7**, 1 (2017).
[20] L. P. Gorkov and V. Z. Kresin, Reviews of Modern Physics **90**, 011001 (2018).
[21] M. Kostrzewa, K. Szczęśniak, A. Durajski, and R. Szczęśniak, Scientific Reports **10**, 1 (2020).
[22] A. Bianconi, in *AIP Conference Proceedings*, Vol. 652 (American Institute of Physics, 2003) pp. 13–18.
[23] A. Vittorini-Orgeas and A. Bianconi, Journal of superconductivity and novel magnetism **22**, 215 (2009).
[24] F. Palumbo, A. Marcelli, and A. Bianconi, Journal of Superconductivity and Novel Magnetism **29**, 3107 (2016).
[25] A. Bianconi and T. Jarlborg, Novel Superconducting Materials **1** (2015).
[26] A. Bianconi and T. Jarlborg, EPL (Europhysics Letters) **112**, 37001 (2015).
[27] T. Jarlborg and A. Bianconi, Scientific reports **6**, 24816 (2016).
[28] Y. Quan and W. E. Pickett, Physical Review B **93**, 104526 (2016).
[29] T. X. Souza and F. Marsiglio, International Journal of Modern Physics B **31**, 1745003 (2017).
[30] F. Capitani, B. Langerome, J.-B. Brubach, P. Roy, A. Drozdov, M. Eremets, E. Nicol, J. Carbotte, and T. Timusk, Nature physics **13**, 859 (2017).
[31] U. Fano, Il Nuovo Cimento (1924-1942) **12**, 154 (1935).
[32] U. Fano, Physical Review **124**, 1866 (1961).
[33] I. Lifshitz *et al.*, Sov. Phys. JETP **11**, 1130 (1960).
[34] G. Volovik, Low Temperature Physics **43**, 47 (2017).
[35] G. Volovik and K. Zhang, Journal of Low Temperature Physics **189**, 276 (2017).
[36] G. E. Volovik, Physics-Uspekhi **61**, 89 (2018).
[37] K. Kugel, A. Rakhmanov, A. Sboychakov, N. Poccia, and A. Bianconi, Physical Review B **78**, 165124 (2008).
[38] A. Bianconi, N. Poccia, A. Sboychakov, A. Rakhmanov, and K. Kugel, Superconductor Science and Technology **28**, 024005 (2015).
[39] A. Perali, A. Bianconi, A. Lanzara, and N. L. Saini, Solid State Communications **100**, 181 (1996).
[40] A. Valletta, A. Bianconi, A. Perali, and N. Saini, Zeitschrift für Physik B Condensed Matter **104**, 707 (1997).
[41] A. Bianconi, A. Valletta, A. Perali, and N. L. Saini, Physica C: Superconductivity **296**, 269 (1998).

[42] A. Bianconi, Journal of Physics and Chemistry of Solids **67**, 567 (2006).
[43] A. Perali, D. Innocenti, A. Valletta, and A. Bianconi, Superconductor Science and Technology **25**, 124002 (2012).
[44] A. Bianconi, S. Agrestini, G. Bianconi, D. Di Castro, and N. Saini, Journal of alloys and compounds **317**, 537 (2001).
[45] A. Perali, P. Pieri, L. Pisani, and G. Strinati, Physical review letters **92**, 220404 (2004).
[46] A. Perali, P. Pieri, and G. Strinati, Physical review letters **93**, 100404 (2004).
[47] A. Bianconi, Journal of Superconductivity **18**, 625 (2005).
[48] D. Innocenti, N. Poccia, A. Ricci, A. Valletta, S. Caprara, A. Perali, and A. Bianconi, Physical Review B **82**, 184528 (2010).
[49] D. Innocenti, S. Caprara, N. Poccia, A. Ricci, A. Valletta, and A. Bianconi, Superconductor Science and Technology **24**, 015012 (2010).
[50] G. Bianconi, Physical Review E **85**, 061113 (2012).
[51] D. Innocenti and A. Bianconi, Journal of superconductivity and novel magnetism **26**, 1319 (2013).
[52] A. Bianconi, Nature Physics **9**, 536 (2013).
[53] M. V. Mazziotti, A. Valletta, G. Campi, D. Innocenti, A. Perali, and A. Bianconi, EPL (Europhysics Letters) **118**, 37003 (2017).
[54] N. Pinto, C. Di Nicola, A. Trapananti, M. Minicucci, A. Di Cicco, A. Marcelli, A. Bianconi, F. Marchetti, C. Pettinari, and A. Perali, Condensed Matter **5**, 78 (2020).
[55] M. V. Mazziotti, A. Valletta, R. Raimondi, and A. Bianconi, Phys. Rev. B **103**, 024523 (2021).
[56] A. Bianconi, D. Innocenti, A. Valletta, and A. Perali, in *J. Phys.: Conf. Ser.*, Vol. 529 (IOP Publishing, 2014) p. 012007.
[57] M. V. Mazziotti, N. Scopigno, M. Grilli, and S. Caprara, Condensed Matter **3**, 37 (2018).
[58] H. Feshbach, Annals of Physics **19**, 287 (1962).
[59] H. Feshbach, Nuclear Physics A **409**, 423 (1983).
[60] H. Feshbach, Niels Bohr: Physics and the World , 117 (2014).
[61] A. E. Miroshnichenko, S. Flach, and Y. S. Kivshar, Reviews of Modern Physics **82**, 2257 (2010).
[62] A. Bianconi, H. Petersen, F. C. Brown, and R. Bachrach, Physical Review A **17**, 1907 (1978).
[63] A. Bianconi, Applications of Surface Science **6**, 392 (1980).
[64] A. Bianconi, M. Dell'Ariccia, P. Durham, and J. Pendry, Physical Review B **26**, 6502 (1982).
[65] H. Suhl, B. Matthias, and L. Walker, Physical Review Letters **3**, 552 (1959).
[66] V. Moskalenko, Fiz. Metal. Metalloved **8**, 2518 (1959).
[67] J. Kondo, Progress of Theoretical Physics **29**, 1 (1963).
[68] M. V. Mazziotti, T. Jarlborg, A. Bianconi, and A. Valletta, EPL (Europhysics Letters) **134**, 17001 (2021).
[69] M. Zwierlein, C. Stan, C. Schunck, S. Raupach, A. Kerman, and W. Ketterle, Physical Review Letters **92**, 120403 (2004).
[70] J. Zhang, E. Van Kempen, T. Bourdel, L. Khaykovich, J. Cubizolles, F. Chevy, M. Teichmann, L. Tarruell, S. Kokkelmans, and C. Salomon, Physical Review A **70**, 030702 (2004).
[71] Y. Uemura, G. Luke, B. Sternlieb, J. Brewer, J. Carolan, W. Hardy, R. Kadono, J. Kempton, R. Kiefl, S. Kreitzman, *et al.*, Physical review letters **62**, 2317 (1989).
[72] F. Pistolesi and G. C. Strinati, Physical Review B **49**, 6356 (1994).
[73] S. Agrestini, N. Saini, G. Bianconi, and A. Bianconi, Journal of Physics A: Mathematical and General **36**, 9133 (2003).
[74] R. Szczesniak and A. Durajski, Solid State Communications **249**, 30 (2017).
[75] R. Szczesniak and A. P. Durajski, Scientific reports **8**, 1 (2018).
[76] A. Perali, A. Valletta, G. Bardeiloni, A. Bianconi, A. Lanzara, and N. Saini, Journal of Superconductivity **10**, 355 (1997).
[77] L. Testardi, Reviews of Modern Physics **47**, 637 (1975).
[78] A. Bianconi, S. Della Longa, C. Li, M. Pompa, A. Congiu-Castellano, D. Udron, A. Flank, and P. Lagarde, Physical Review B **44**, 10126 (1991).
[79] A. Bianconi, N. Saini, A. Lanzara, M. Missori, T. Rossetti, H. Oyanagi, H. Yamaguchi, K. Oka, and T. Ito, Physical Review Letters **76**, 3412 (1996).
[80] A. Bianconi, M. Lusignoli, N. Saini, P. Bordet, Å. Kvick, and P. Radaelli, Physical Review B **54**, 4310 (1996).
[81] V. A. Gavrichkov, Y. Shanko, N. G. Zamkova, and A. Bianconi, The journal of physical chemistry letters **10**, 1840 (2019).
[82] A. Bianconi, N. L. Saini, S. Agrestini, D. Di Castro, and G. Bianconi, International Journal of Modern Physics B **14**, 3342 (2000).
[83] D. Di Castro, G. Bianconi, M. Colapietro, A. Pifferi, N. Saini, S. Agrestini, and A. Bianconi, The European Physical Journal B-Condensed Matter and Complex Systems **18**, 617 (2000).
[84] L. Barba, G. Chita, G. Campi, L. Suber, E. M. Bauer, A. Marcelli, and A. Bianconi, Journal of Superconductivity and Novel Magnetism **31**, 703 (2018).
[85] E. Bauer, C. Paul, S. Berger, S. Majumdar, H. Michor, M. Giovannini, A. Saccone, and A. Bianconi, Journal of Physics: Condensed Matter **13**, L487 (2001).
[86] S. Agrestini, D. Di Castro, M. Sansone, N. Saini, A. Saccone, S. De Negri, M. Giovannini, M. Colapietro, and A. Bianconi, Journal of Physics: Condensed Matter **13**, 11689 (2001).
[87] A. Bianconi, D. Di Castro, S. Agrestini, G. Campi, N. Saini, A. Saccone, S. De Negri, and M. Giovannini, Journal of Physics: Condensed Matter **13**, 7383 (2001).
[88] S. Agrestini, C. Metallo, M. Filippi, L. Simonelli, G. Campi, C. Sanipoli, E. Liarokapis, S. De Negri, M. Giovannini, A. Saccone, *et al.*, Physical Review B **70**, 134514 (2004).
[89] D. Di Castro, S. Agrestini, G. Campi, A. Cassetta, M. Colapietro, A. Congeduti, A. Continenza, S. De Negri, M. Giovannini, S. Massidda, *et al.*, EPL (Europhysics Letters) **58**, 278 (2002).
[90] A. Ricci, N. Poccia, G. Ciasca, M. Fratini, and A. Bianconi, Journal of superconductivity and novel magnetism **22**, 589 (2009).
[91] A. Ricci, N. Poccia, B. Joseph, L. Barba, G. Arrighetti, G. Ciasca, J.-Q. Yan, R. W. McCallum, T. A. Lograsso, N. Zhigadlo, *et al.*, Physical Review B **82**, 144507 (2010).

[92] A. A. Kordyuk, Low Temperature Physics **44**, 477 (2018).

[93] Y. V. Pustovit and A. Kordyuk, Low Temperature Physics **42**, 995 (2016).

[94] A. Guidini, L. Flammia, M. V. Milošević, and A. Perali, Journal of Superconductivity and Novel Magnetism **29**, 711 (2016).

[95] M. Cariglia, A. Vargas-Paredes, M. M. Doria, A. Bianconi, M. V. Milošević, and A. Perali, Journal of Superconductivity and Novel Magnetism **29**, 3081 (2016).

[96] M. M. Doria, M. Cariglia, and A. Perali, Physical Review B **94**, 224513 (2016).

[97] A. Bussmann-Holder, J. Köhler, M.-H. Whangbo, A. Bianconi, and A. Simon, Novel Superconducting Materials **1** (2016).

[98] D. Valentinis, D. Van Der Marel, and C. Berthod, Physical Review B **94**, 024511 (2016).

[99] A. Bussmann-Holder, J. Kohler, A. Simon, M.-H. Whangbo, A. Bianconi, and A. Perali, Condensed Matter **2**, 24 (2017).

[100] A. Bussmann-Holder, H. Keller, A. Simon, and A. Bianconi, Condensed Matter **4**, 91 (2019).

[101] A. V. Chubukov and D. Mozyrsky, Low Temperature Physics **44**, 528 (2018).

[102] L. Salasnich, A. Shanenko, A. Vagov, J. A. Aguiar, and A. Perali, Physical Review B **100**, 064510 (2019).

[103] M. Y. Kagan and A. Bianconi, Condensed Matter **4**, 51 (2019).

[104] H. Tajima, A. Perali, and P. Pieri, Condensed Matter **5(1)** (2020).

[105] A. Vargas-Paredes, A. Shanenko, A. Vagov, M. Milošević, and A. Perali, Physical Review B **101**, 094516 (2020).

[106] A. Bianconi, European Patent EP0733271 Sept **25** (1996).

[107] A. Bianconi, "Process of increasing the critical temperature tc of a bulk superconductor by making metal heterostructures at the atomic limit," (2001), uS Patent 6,265,019.

[108] A. Bianconi, Solid state communications **89**, 933 (1994).

[109] A. Bianconi, D. Innocenti, and G. Campi, Journal of Superconductivity and Novel Magnetism **26**, 2585 (2013).

[110] A. Bianconi, in *J. Phys.: Conf. Ser.*, Vol. 449 (IOP Publishing, 2013) p. 012002.

[111] G. Masella, A. Angelone, F. Mezzacapo, G. Pupillo, and N. V. Prokof?ev, Physical review letters **123**, 045301 (2019).

[112] H. Isobe and L. Fu, Physical Review Research **1**, 033206 (2019).

[113] A. Bianconi, A. Valletta, A. Perali, and N. Saini, Solid State Communications **102**, 369 (1997).

[114] A. Migdal, Sov. Phys. JETP **7**, 996 (1958).

[115] L. Simonelli, V. Palmisano, M. Fratini, M. Filippi, P. Parisiades, D. Lampakis, E. Liarokapis, and A. Bianconi, Physical Review B **80**, 014520 (2009).

[116] K. Ochi, H. Tajima, K. Iida, and H. Aoki, arXiv preprint arXiv:2107.13805 (2021).